The Journal of the Korean Society of
Coastal and Ocean Engineers
Vol. 6, No. 3, pp. 309~325, September 1994

A Numerical Modeling Study on the Seasonal Variability in the Gulf of Alaska
알라스카 灣의 季節變化에 대한 數値模型 實驗

In Kweon Bang* and Zygmunt Kowalik**
方仁權* · 지그문트 코발릭**

Abstract □ Ocean circulation in the Gulf of Alaska is remarkably constant throughout the year despite of being forced by one of the largest seasonal wind stresses in the world. To explain the small seasonal changes in the transport of Alaska Stream, a set of numerical models is employed. First, a diagnostic approach is applied to reproduce circulation from the observed density structure. The results reveals the very small seasonal changes in the Alaska Stream transport. Next, a series of the prognostic models is used: a barotropic model, a flat bottom baroclinic model, and baroclinic model with topography. These models reveal the influence of topography and baroclinicity on the ocean's response to the seasonal wind forcing. The intercomparisons of the various model results suggest that the seasonal response of the baroclinic ocean is primary barotropic and the resultant barotropic circulation is weakened by the scattering effect of the bottom topography.

要 旨 : 알라스카 만의 해수순환은 바람응력의 큰 계절적 변동에도 불구하고 큰 변화를 보이지 않는다. 그 역학적 원인을 알아보기 위해 일련의 수치모델 실험을 행하였다. 먼저, 관측밀도장으로부터 구한 진단모델 결과에 의하면 알라스카 난류의 계절적 변동은 거의 없으며, 여러종류의 예보모델 결과에 의하면 해저지형과 경압성이 바람의 계절변동에 대한 해양반응에 영향을 미침을 보여준다. 모델 결과의 비교에 의해 경압해양의 바람의 계절변동에 대한 반응은 주로 순압성이며 순압 해수순환은 해저지형의 분산효과에 의해 약해지기 때문에 해수순환의 계절적 변동이 거의 나타나지 않는다.

1. INTRODUCTION

Long-term mean transport of the western boundary current can be estimated by the zonal integration of mean wind stress curl, i.e., the Sverdrup balance can be used to estimate the mean transport (for example, Warren and Owens 1988). However, the seasonal variation cannot be explained by the integration of the seasonal wind stress curl. For example, the observed transport of the Florida current is maximum in summer with an annual cycle of 4 Sv while the integration of the seasonal wind stress curl predicts maximum in winter with an annual variation of 15 Sv (Anderson and Corry 1985 b).

Seasonal migration of the Aleutian Low and Pacific High causes a large seasonal fluctuation in the wind stress pattern in the Gulf of Alaska. Spatial distributions of the long-term monthly mean wind stress curl averaged from 1946 to 1988 (Fig. 1) show the large seasonal cycle in the gulf. In winter the Aleutian Low is strong and the total wind-driven transports into the gulf should reach about 20 Sv. In summer the Pacific High dominates and the transport is only 5 Sv (Reed *et al.* 1980). Musgrave *et al.* (1992) also report an expected seasonal transport variation of about 40 Sv near Cook Inlet based on the geostrophic current from the wind

*韓國海洋研究所 海洋物理研究部 (Physical Oceanography Division, Korea Ocean Research and Development Institute, Ansan P.O. Box 29, 425-600, Korea)
**알라스카 대학 해양연구소 (Institute of Marine Science, University of Alaska Fairbanks, Fairbanks, Alaska 99701, U.S.A.)

stress curl. It is surprising therefore that the circulation pattern remains almost constant despite large fluctuations in the atmospheric conditions over the gulf (Favorite *et al.* 1976). Reed *et al.* (1980) found no clear evidence of seasonal cycle in the transport of the Alaska Stream (Reed 1968) and sea level (Reid and Mantyla 1976) while Royer (1981) estimated the seasonal variation in the transport of the Alaska Stream near Kodiak Island to be about 13% of the mean transport. An explanation of this small seasonal variation in the gulf is the objective of this study.

The predicted seasonal variation in the transport of the western boundary current by the wind stress curl is far larger than the observations and the predicted phase is not consistent with the observations. Therefore, it is clear that the ocean responds to the seasonal fluctuations in the wind with different dynamics from the Sverdrup dynamics which is successful in explaining the annual mean circulation.

There are several theoretical and numerical works on the oceanic response to the time-dependent forcing. Veronis and Stommel (1956) first considered the ocean response to the time-dependent wind forcing and concluded that in the middle and high latitudes the ocean response is mainly barotropic. At low latitude, Lighthill (1969) showed that the relatively fast group velocity of the baroclinic Rossby wave near the equator is responsible for the reversal of the Somali Current, which takes place within a month from the change of the seasonal monsoon. In a series of papers, Anderson and Gill (1975) developed a two-layer one-dimensional model to study the barotropic and baroclinic responses of the ocean to the wind forcing, Anderson and Killworth (1977) include the effect of topography, and Anderson and Corry (1985a) applied time-dependent wind forcing to their model. From these studies, Anderson and Corry (1985a) concluded that the propagation time of the baroclinic Rossby wave from a generation point to the western boundary is important in determining whether the western boundary current will respond barotropically or baroclinically. According to Anderson and Corry (1985a and b), the response of the western boundary current to the annual forcing is barotropic at the middle and high latitudes. Sverdrup balance holds in the interior only after the passage of baroclinic Rossby waves.

Following these theoretical and numerical works, Anderson and Corry (1985b) used a two-layer model in the North Atlantic and Greatbatch and Goulding (1989) used a vertically integrated linear model in the North Pacific to see if a barotropic response alone can explain the observed seasonal variability. The results showed that the predicted seasonal variation in Florida Current by Anderson and Corry (1985b) was in phase with observation, but their amplitude was several factors smaller. Greatbatch and Goulding (1989) also reached at the similar conclusion for the Kuroshio. To explain the discrepancy of the model results with the observations, Anderson and Corry (1985b) mentioned baroclinic Kelvin waves and topographic Rossby waves as possible contributors.

Numerical modeling was employed to understand and explain why there is little to no seasonal variability in the transport of the Alaska Stream even though it is found under one of the largest seasonal fluctuation in the atmospheric condition in the world. To achieve this goal, a series of numerical experiments have been carried out. These numerical models vary in complexity ranging from a diagnostic model to a prognostic, time dependent model with bottom topography. A short description of the numerical models, boundary conditions and initial conditions are given in Section 2. A diagnostic model is used to reproduce a circulation expected from observed density structure in the Gulf of Alaska (Section 3). Integrations are done over each season and results are discussed in terms of annual mean circulation and seasonal variability.

In Section 4, the Gulf of Alaska is assumed homogeneous and effect of topography on the oceanic response to seasonal wind forcing is discussed. This barotropic model follows a theory of Anderson and Corry (1985a) which predicts that the seasonal response of the western boundary current in middle and high latitudes is mainly barotropic. In Section 5, flat-bottom and topography cases are employed to study the baroclinic ocean response to the seasonal forcing. Discussion and conclusions are given

in Section 6.

2. NUMERICAL MODEL

Semtner's version (1974) of Bryan's (1969) primitive equation model is used in this study and detailed descrptions for the boundary conditions and forcing are given in the companion paper (Bang and Kowalik 1994).

Maximum positive wind stress curl is about 3×10^{-8} dyn/cm^3 and is located at 58° N, 140° W (Fig. 1). In general, the wind stress curl used in this study is higher in the region north of 55° N and lower to the south of 55° N compared to Willebrand (1978). Interestingly, the seasonal variation of the wind stress curl is large in the northeast corner of the gulf where a large annual mean wind stress curl is also found. Monthly mean wind stress curls for selected months (Fig. 2) also illustrates the temporal variabilities of the wind stress curl.

In the diagnostic model, temperature and salinity data of Levitus (1982) were used as the observation data. From a given density field, a current field can be constructed by several methods. The traditional dynamic method, although quite simple dynamically and easy to use, produces reasonable results with an appropriate choice of level of no motion.

The archive of observations now allows another type of computation to construct the velocity field. Pioneering calculations using the observed density field have been made by Sarkisyan and coworkers (1966, 1970, 1971). They used a modified set of the steady-state equations of motion to compute the velocity field for the Atlantic Ocean. However, Holland and Hirshmann (1972) integrated the Bryan (1969) time-dependent primitive equation model while holding the density fixed in time. This type of computation is attractive because 1) no modifications which may cause some loss of dynamics are made, 2) the spin-up time is only on the order of months, which can be compared to a thousand years of prognostic model and 3) there is no uncertainty due to the level of no motion like dynamic

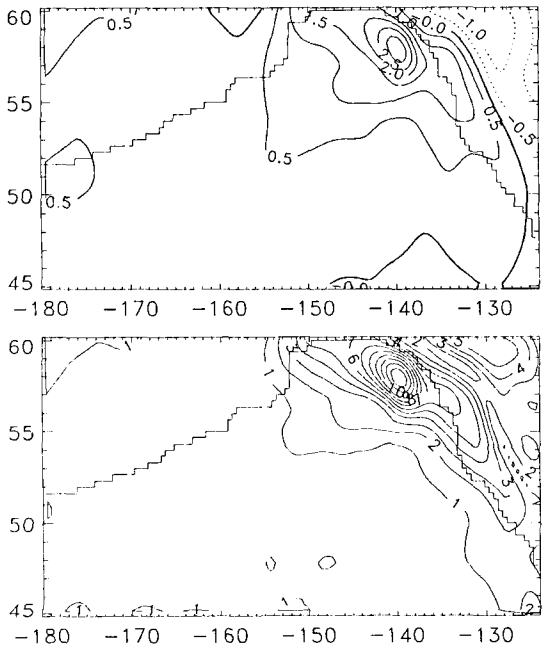

Fig. 1. Annual mean wind stress curl (upper) and seasonal range of the wind stress curl (lower). Unit is 1×10^{-8} dyn/cm^3.

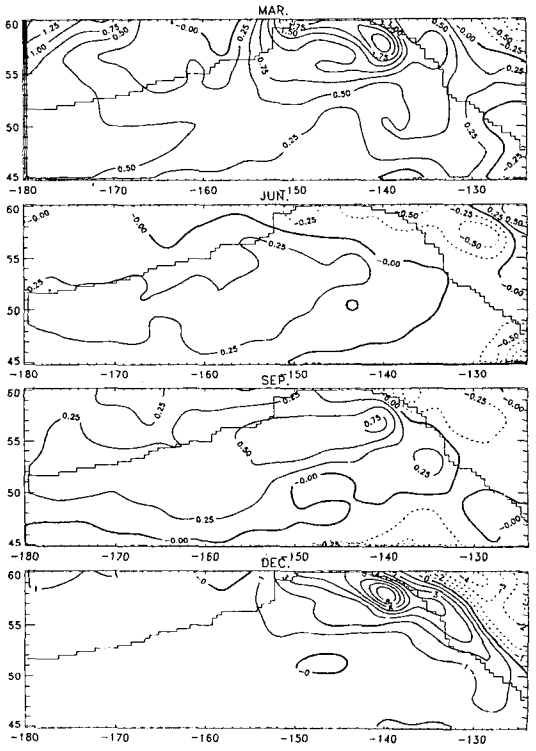

Fig. 2. Monthly mean wind stress curl (10^{-8} dyn/cm^3) in March, June, September, and December. Solid contour lines are for positive wind stress curl.

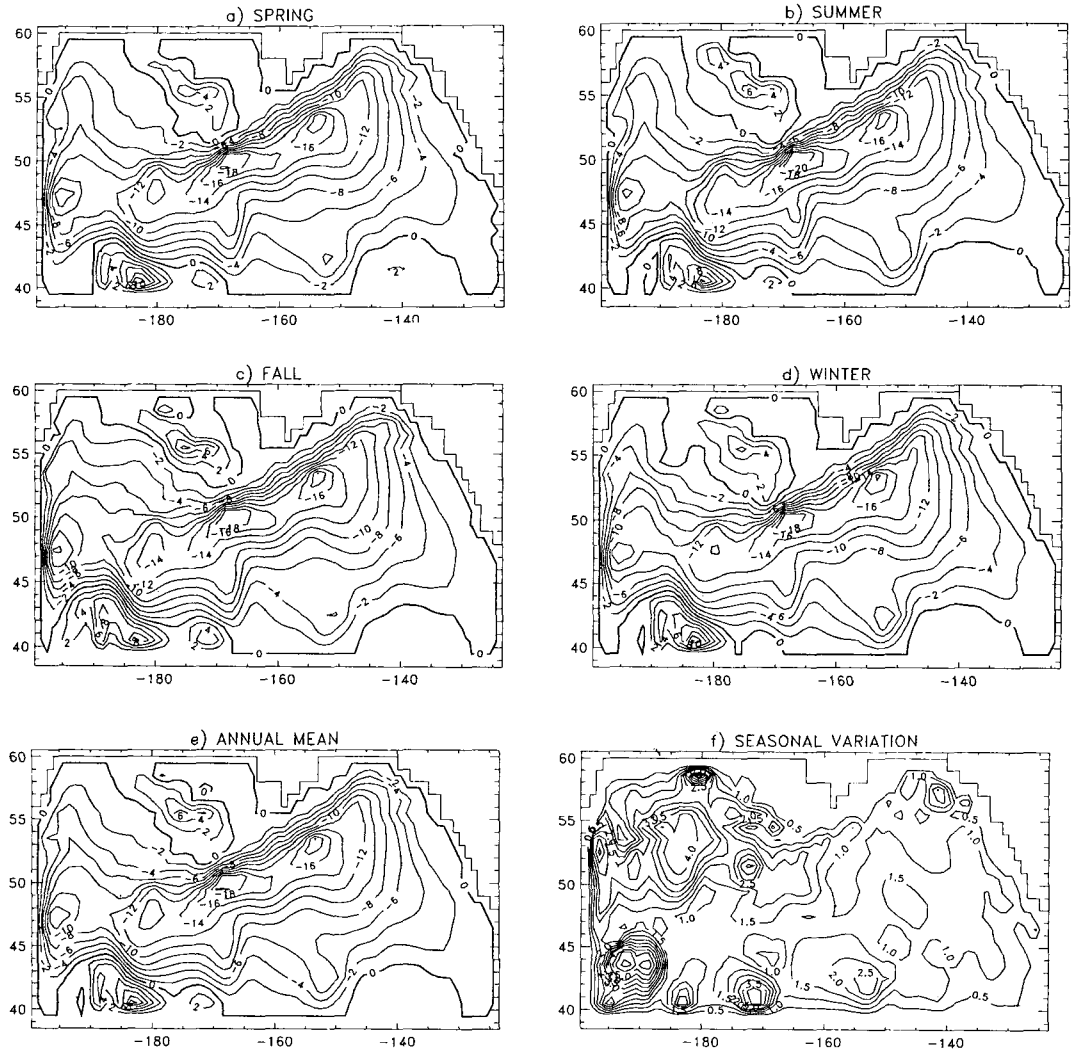

Fig. 3. Stream function from the diagnostic model in: a) spring, b) summer, c) fall, d) winter, and e) annual mean and f) seasonal range of the stream function.

method. In fact, Holland and Hirshmann (1972) were quite successful in reproducing major features in the North Atlantic circulation.

We have applied the same computations as those used by Holland and Hirshmann (1972) for the mean and seasonal circulation in the Gulf of Alaska. The mean circulation is compared with the observed circulation and the seasonal variation in the gulf is extracted.

3. DIAGNOSTIC MODEL RESULTS

For the diagnostic model, 1° horizontal resolution and 32 vertical levels were used. The density data from Levitus (1982) were applied in computation and several sets of data were used: yearly averages and four seasons.

Biharmonic diffusion is used with the coefficient of -4×10^{21} cm^4/sec. The model ocean is closed at 40° N and 160° E and the Bering Sea is included in the computation. At the southern and western boundaries, which are not natural boundaries, a slip boundary condition is used. A no-slip boundary co-

ndition is applied at the land-sea boundary.

Integration from the initially motionless state with 1 hour time step is performed for one month. This leads to a quasi stationary state. Wind stress was not applied since the observed density field already contains wind information (Holland and Hirschman 1972). Holland and Hirschman (1972) report only 5% decrease in Gulf Stream transport when wind is not included in the model and they conclude that the pressure torque associated with the bottom topography is the main vorticity input.

The stream functions of the vertically integrated transport (Fig. 3) show no significant differences in the circulation pattern from season to season so that any season can be selected for a discussion of the mean circulation in the Gulf of Alaska. A cyclonic gyre occupies most of the model region extending from the western artificial boundary at 160° E to the coast of America and small anticyclonic gyres are present near the southern artificial boundary and in the eastern Bering Sea. The southwestward flowing Alaska Stream is identifiable as a narrow and intense current from 145° W to the dateline. The current width is about 250 km and the volume transport is about 12 Sv near Kodiak Island. As the Alaska Stream flows downstream, the transport increases to about 20 Sv at 154° W. But the transport decreases downstream of this longitude until it begins to increase again around 160° W. This pattern of increase and decrease in the transport of the Alaska Stream is due to the low values in the stream function (a cyclonic gyre has negative values of the stream function) located just south of the Alaska Stream. They are found at 154° W, 170° W and 180° and recirculations occur in the first half region between two lows.

Since the total transport is the transport from surface to bottom, it is not appropriate for a comparison with the geostrophic transport calculated from observations which are usually referenced to 1,000 or 1,500 db. Furthermore, the contribution by the slow deep circulation, which is affected strongly by topography, is contained in the stream function (Holland and Hirschman 1972). For these reasons, the flow is depicted using particle tracks released at every grid point. Mean horizontal velocity of the upper 1,000 m in fall is used to compute positions of each particle in the horizontal plane at regular interval using the linear interpolation for the velocity (Fig. 4).

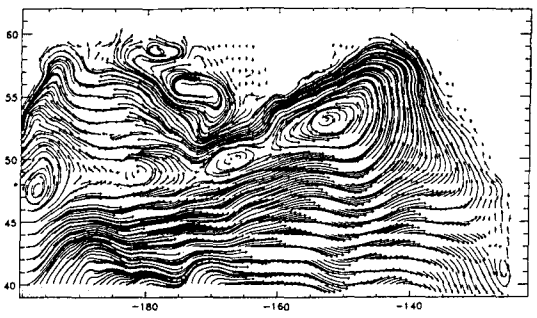

Fig. 4. Particle tracks followed for one year show the fall diagnostic circulation in the upper 1,000 m (the position is computed every 5 days).

The major circulation features of the Northeast Pacific (Fig. 4) are identifiable: the Subarctic Current and its bifurcation into Alaska Current and California Current, the Alaska Stream, and recirculation. It is also interesting to note that the currents near the artificial boundaries behave as if there were no boundaries, i.e., the currents near these boundaries show strong inflow and outflow perpendicular to them.

Observations of the deep circulation here below the wind-driven surface circulation are rare. Results from this diagnostic computation can provide a picture of deep circulation within limitations of the model. Particle tracks for depths from 1,000 m to 4,000 m are computed at 1,000 m intervals (here only particle plot in 2,000-3,000 m is shown in Fig. 5). Particles are followed for one year for 1,000 m-2,000 m depths and for two years in the deeper depth ranges. The first thing to note is the absence of the eastward flowing Subarctic Current below 2,000 m. In general, there is a northward flowing current in the eastern part of the gulf, east of about 150° W and westward flowing current to the west of 150° W. This northward flowing current, the Alaska Current, feeds the Alaska Stream. West of 170° W, the extension of the Alaska Stream, is joined by another westward flowing current and they turn into a southerly flow west of their merger.

Support for the pattern of the diagnostic model's

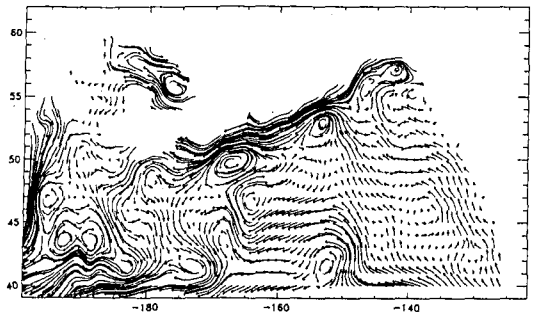

Fig. 5. Particle tracks followed for two years show the fall diagnostic circulation in 2,000-3,000 m (the position is computed every 10 days).

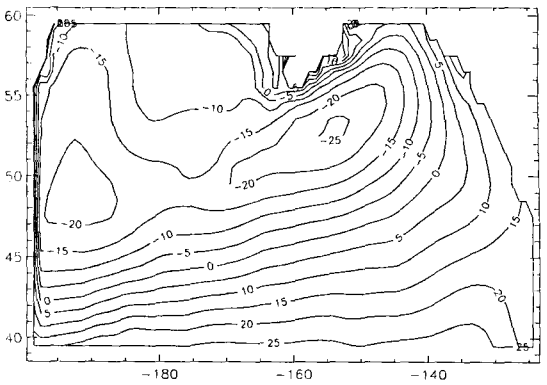

Fig. 6. Distribution of the sea levels (in cm) in summer defined from diagnostic model.

deep circulation can be found in Reid and Arthur (1975). Their maps of geopotential anomalies at 2, 500 db relative to 3,500 db and 3,000 db relative to 4,000 db show a northward flowing current near the coast of America and westward flowing current to the west. Although these flows are relative, geostrophic currents, their agreement with the model results is encouraging.

One conspicuous feature that distinguishes the model's deep circulation (Fig. 5) from that of the surface is the appearance of the small closed circulations or eddies of 200-500 km in size. They are most clearly defined in the deepest depth ranges but they are not related to the mesoscale topographic features such as seamounts except for the one at 170° E, 44° N which might be due to Emperor Seamount chain. In fact, no other seamount is resolved by 1° resolution of this model. Two cyclonic eddies located offshore of the Alaska Stream at 153° W and 167° W are related to the center of the Alaska gyre and the recirculation in the surface layers. To the south of these eddies there are four more eddies between 150° W and 180° (Fig. 5) of unknown origin. One possible cause of these eddies is the change of model depth in this region. Hydrographic measurements are necessary for the comparison with the model results. These eddies remain to be studied further.

An estimate of the seasonal variability in the Gulf of Alaska was made from the diagnostic computation to compare with observations and other experiments of this study. The seasonal variability of the diagnostic circulation is defined as the range of variation of the stream function over four seasons.

Our discussion will focus on the region east of 165° W and north of 45° N. The seasonal range of variation is less than 2 Sv except for about 2.5 Sv in the northeast corner of the gulf. The seasonal range is about 0.5-2 Sv along the Alaska Stream from 145° W to 165° W.

A seasonal shift of the Alaska gyre is observed in the numerical model results of Cummins (1989). The Alaska gyre shifts 150-250 km offshore from the west coast of North America in July and resumes its position in January. Cummins (1989) further suggested that the interannual gyre shift (Royer and Emery 1987) is simply an amplification of this regular seasonal variation. However, no seasonal shift of the Alaska gyre is observed in the diagnostic model results of this study. Instead, only a slight intensification of the westward flowing current between 140° W and 150° W is noticeable in fall and winter.

Sea level is a good parameter that can be used to compare the model results with the observation (dynamic topography). The sea level is not an explicit variable computed during the integration in this model but it is possible to compute sea level from the pressure gradient. The distribution of the sea level at the surface (actually at 10 m depth) shows the surface circulation pattern and the lowest sea level is found at 53° N, 153° W (Fig. 6). If the sea levels −15 cm and −20 cm are respectively defined as the main axis and the offshore limit of the Alaska Stream between 145° W and 175° W

the sea level change across the Alaska Stream is 15-20 cm.

4. SEASONAL BAROTROPIC MODEL

In this section, a barotropic model is used to investigate the influences of bottom topography on the ocean response to the seasonal forcing in the Gulf of Alaska. In the eastern gulf, the lines of constant barotropic potential vorticity f/H are almost parallel to the coastline of North America so that one can expect that barotropic Rossby waves propagate northwestward instead of westward. If this is true, wind changes in the Alaska Current region over the continental slope offshore of North America would be important in the seasonal variation of the Alaska Stream transport.

The model configuration is 30′ (zonal)×20′ (meridional)×20 layers. Kodiak Island and Queen Charlotte Island are connected to the land and no passages into the Bering Sea are resolved (Fig. 9). The density (constant temperature at 4℃, constant salinity at 33 psu) is constant. The barotropic ocean with no initial motion is forced by a seasonally varying wind stress. Each month has 30 days. Both horizontal components of the wind stress are first decomposed into harmonics. The new wind stress to be used for the actual wind forcing is reconstructed at every timestep from the mean, annual, and semi-annual harmonics. Integration is done for 14 months. The bottom topography is fairly well defined by the 20 layers (Fig. 9).

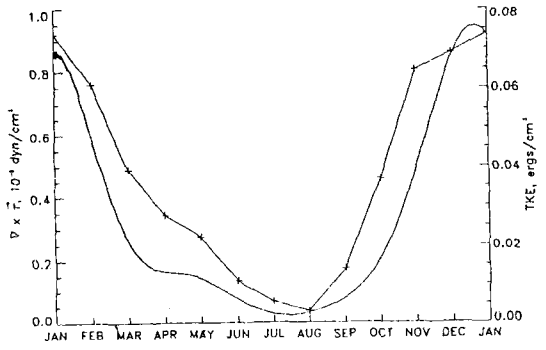

Fig. 7. Basin-averaged kinetic energy (ergs/cm^3) of the seasonal barotropic model and the average wind stress curl over the entire model domain (+).

The biharmonic coefficient in the interior is -4×10^{19} cm^4/sec for momentum. The Laplacian coefficient used in the sponge layer near the western boundary is 1×10^8 cm^2/sec. A linear bottom friction is also used with the damping time scale of 5 days. Horizontal boundary conditions are same as in the diagnostic model, that is, a no-slip condition at the land-sea boundary and a slip boundary condition at the artificial wall.

The spin-up time of the seasonal barotropic model from the initial state of no motion is 5-10 days. The basin-averaged kinetic energy shows a large seasonal variation with its maximum of 0.08 ergs/cm^3 in January and almost zero in July (Fig. 7) and is in phase with the wind stress curl. As is evident from the maximum kinetic energy (0.08 ergs/cm^3), the kinetic energy level is low. The mean circulation shows a cyclonic gyre but the mean transport is only about 1 Sv in the Alaska Stream (Fig. 8).

The semi-closed cyclonic gyre sitting between 170° W and 150° W south of 50° N consists of a

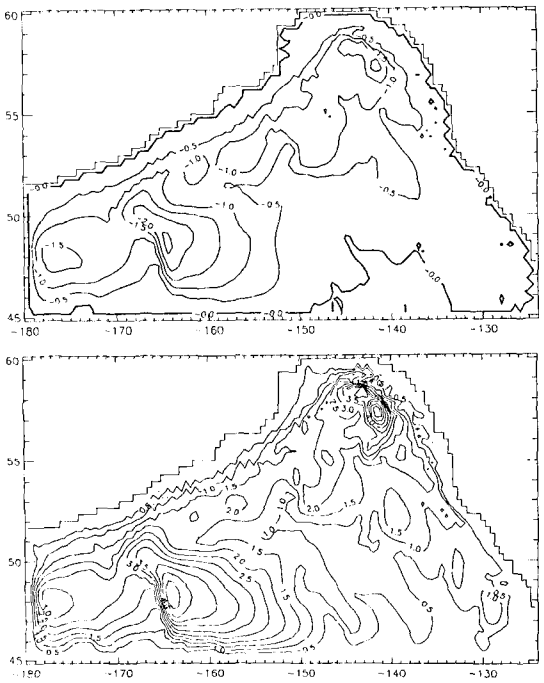

Fig. 8. Annual mean (upper) and seasonal range (lower) of the stream function (in Sv) from the barotropic model.

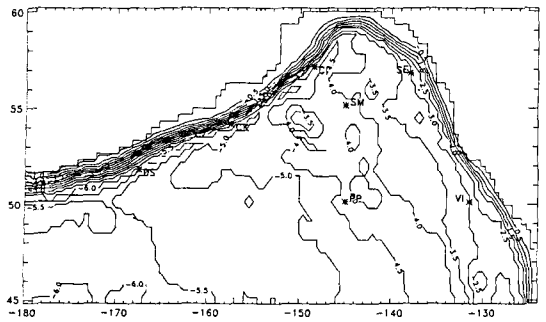

Fig. 9. Topography defined by number of layers. Seven monitoring points are marked by asterisk (VI: Vancouver Island, PP: Papa, CI: Cook Inlet, SE: Sitka Eddy, SM: Seamount, CK: Chirikof Island, and DS: Downstream)

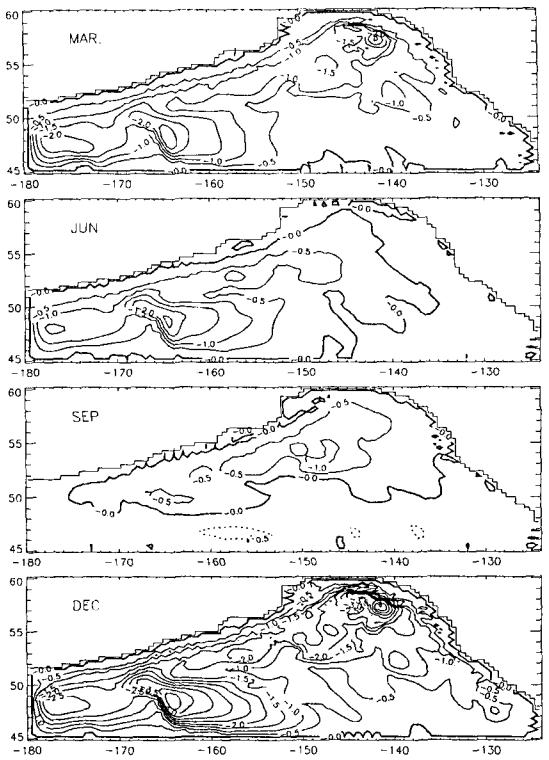

Fig. 10. Stream functions of barotropic transport at the middle of March, June, September, and December.

western boundary current which flows southward along the 5,500 m isobath, a northward interior flow between two the isobaths of 5,500 and 5,000 m, and zonal flows connecting these meridional flows (Fig. 8). The 5,500 m isobath where the western boundary current is formed has a large slope normal to it so that the depth decreases suddenly from 6,000 m to 5,500 m (Fig. 8). On each side of the depth discontinuity, there exist large areas of constant depth (5,500 m in the eastern area and 6,000 m in the western area). Separate cyclonic gyres form in each area.

The northward flow in the flat area between 160° W and 150° W is the Sverdrup response to the positive wind stress curl and is returned to the south by the western boundary current. There is no such a depth discontinuity in the Gulf of Alaska and the Aleutian Abyssal Plain is almost of uniform depth. One expects that the Rossby waves actually propagate more or less westward in the Aleutian Abyssal Plain because of its flatness.

In the region east of the 5,000 m isobath the depth decreases to the coast. In this eastern region, the topography is complicated by the presence of seamounts and the interpretation of the circulation in this shallow region is not straightforward. The time-dependent forcing also makes it difficult to detect any propagation of the signals. However, another computation forced by the annual mean wind shows a northwestward propagation of the barotropic Rossby waves in the region east of 150° W as can be expected by the dominance of H in the potential vorticity f/H.

Interestingly, the spatial distribution of the seasonal range (Fig. 8) is similar in pattern to that of the mean circulation. Large seasonal ranges are found in the region with large mean transports and vice versa. The fast response time (5-10 days) implies that the energy input by the wind forcing propagates relatively fast and the time-dependent wind forcing has little effect on the propagation. If this is true, the final monthly circulation would differ little whether the model is forced by the time-dependent seasonal wind stress or by the time-independent monthly wind stress. Thus, the seasonal range of the seasonal barotropic model which is defined by the difference between the maximum and minimum values of the stream functions over one year period can also be estimated from the monthly circulation forced by the strongest positive wind stress curl and the strongest negative wind stress curl.

Greatbatch and Goulding (1989) also noted similar results in the North Pacific and attributed it to the nearly zonal topography in the North Pacific, which does not block and detour the westward propagation of barotropic Rossby wave.

Comparison of the monthly mean circulation (Fig. 10) with the wind stress curl (Fig. 2) provides more evidence for the close relationship between the ocean response and the wind forcing. There is a change in the position of the zero stream function line over the year. The cyclonic gyre is strongest in oceanic fall (December) and covers the entire model domain. In spring (June), the cyclonic gyre has shifted westward and in summer (September), the gyre has shifted northward. These shifts of gyre are the responses to the change of the wind stress curl pattern. The annual mean position of the zero wind stress curl line lies along about 45° N in the ocean though it becomes roughly parallel to the coastline on the land over North America (Fig. 1). The position of the zero line oscillates throughout the year (Fig. 2) and the largest westward shift of the zero line occurs in spring (June) and the largest northward shift occurs in summer (September). These shifts of the zero wind stress curl line are clearly reflected in the monthly mean circulation (Fig. 10) and the positions of the zero wind stress curl line and the zero transport line nearly coincide.

There are interesting similarities in the spatial patterns of the seasonal ranges of barotropic (Fig. 8) and diagnostic models (Fig. 3f). For example, large values in the northeast corner of the model domain and in the region between 160°-170° W south of 50° N and small values between these two regions. Especially, the seasonal range between 145° W and 165° W along the Alaska Steam is about 1-2 Sv and agrees with values from the diagnostic model. This agreement may indicate that the seasonal fluctuation in the transport of the Alaska Stream is primarily barotropic and agrees with the theory of Anderson and Corry (1985a). However, differences in spatial patterns are also noted in some places and they may be due to the mismatch of the density field with the bottom topography in the diagnostic model as explained previously.

In a barotropic ocean, the information imparted by the wind stress curl will be carried away from the interior by barotropic waves only. If the ocean is flat, the barotropic Rossby waves will establish a mean circulation according to the Sverdrup dynamics, that is, the transport in the western boundary current is equal to the interior transport driven by the wind stress curl. On the other hand, if the ocean has bottom topography, the resulting circulation is relatively weak and is strongly controlled by topography. This is because the barotropic Rossby waves no longer propagate in zonal direction and instead, they propagate along the constant lines of f/H so that their destination is not necessarily the western boundary.

The annual mean circulation of the seasonal barotropic model contains a cyclonic gyre as a direct response to the mean positive wind stress curl in the gulf. The energy estimated by the maximum value is only 10% of that of the diagnostic circulation. The spatial patterns of the seasonal range and the annual mean circulation are very similar to each other. The monthly mean circulation also has a similar pattern as the annual mean except for September when the negative wind stress curl is strong. The monthly mean circulation closely follows the seasonal change in the wind stress curl and a westward shift of the cyclonic gyre occurs in oceanic spring (June) and summer (September) when the negative wind stress curl gains the strength.

The seasonal barotropic model predicts 1-2 Sv for the seasonal variation in the transport of the Alaska Stream and this value agrees well with results of the diagnostic model. This agreement leads to the conclusion that the seasonal response of the transport of the Alaska Stream is mainly barotropic. However, a further discussion will be made in Section 5 after the seasonal baroclinic model is considered.

5. SEASONAL BAROCLINIC MODEL

Our proceeding results indicate that the seasonal variability in the gulf, especially in the Alaska Stream, is only about 2 Sv. The role of topography

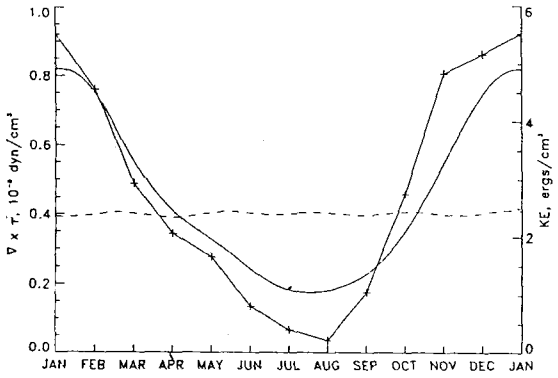

Fig. 11. Basin-averaged kinetic energies (ergs/cm^3) of 10-layer seasonal case (solid) and 10-layer annual mean case (dashed) from year 9-10 and monthly mean wind stress curl (+).

is discussed in the light of the theory of Anderson and Corry (1985a) and the response of the ocean at high latitudes to the seasonal forcing is mainly barotropic which is strongly controlled by topography. As a natural extension of these previous experiments, we simulated the baroclinic ocean response to the seasonal forcing. Two cases are considered: 10-layer case of flat topography and 20-layer case with bottom topography.

5.1 Flat-bottom Case

The basin-averaged kinetic energy (Fig. 11) shows strong annual cycle with maximum in January (about 5 ergs/cm^3) and minimum in July (about 1 erg/cm^3). A most striking feature is the amplitude of the seasonal cycle (about 2 ergs/cm^3) which is comparable in strength to the annual mean circulation (dashed line in Fig. 11 and is about 2.5 ergs/cm^3). Noting that the wind stress curl (solid line with plime) also seasonally fluctuates with an amplitude (about 0.45×10^{-8} dyn/cm^3) comparable to the annual mean wind stress curl, it is clear that the strong seasonal forcing also produces a strong response in a flat-bottom ocean.

A detailed consideration of the energetics is used to explain the seasonal cycle in the kinetic energy. The kinetic energy equations of the total velocity, external mode (defined by the vertical average of the total velocity), and internal mode are derived following Holland (1975).

$$\frac{\partial E}{\partial t}=\iint_{\Sigma}(e+p)V_n d\sigma-\langle \rho g w\rangle+\iint_S \vec{u}\cdot\vec{\tau}_w d\sigma$$
$$-\iint_B \vec{u}\cdot\vec{\tau}_b d\sigma+\langle \vec{u}\cdot\vec{F}\rangle-\left\langle \rho_o \chi\left(\frac{\partial \vec{u}}{\partial z}\right)^2\right\rangle$$
$$=A+G+B+W+D$$

$$\frac{\partial \bar{E}}{\partial t}=-\left\langle \rho_o \vec{u}\cdot\left(\vec{u}\cdot\nabla\vec{u}+w\frac{\partial \vec{u}}{\partial z}\right)\right\rangle-\langle \vec{u}\cdot\overline{\nabla p}\rangle$$
$$+\iint_S \vec{u}\cdot\vec{\tau}_w d\sigma-\iint_B \vec{u}\cdot\vec{\tau}_b d\sigma+\langle \vec{u}\cdot\vec{F}\rangle$$
$$=N_e+B_e+W_e+D_e$$

$$\frac{\partial E'}{\partial t}=N_i+B_i+W_i+D_i$$

where

$$\langle\ \rangle\equiv\iiint\cdot dV$$

$$\overline{(\ )}\equiv\frac{1}{H}\int_{-H}^{0}\cdot dz$$

$$E=\frac{\rho_o}{2}\langle \vec{u}\cdot\vec{u}\rangle$$

$$E=\frac{\rho_o}{2}\langle \vec{u}\cdot\vec{u}\rangle$$

$$E'=\frac{\rho_o}{2}\langle \vec{u}'\cdot\vec{u}'\rangle$$

Σ is the surrounding surfaces of the integration domain including the ocean surface S and the ocean bottom B. V_n is the inward positive normal velocity on the surface and σ is the surface element. In the first equation, the first surface integral on the RHS represents the flux of the total kinetic energy (A) and the pressure work (G) through the boundaries. The wind effect is denoted by W and dissipation (the last three terms) by bottom friction, horizontal friction ($\vec{F}$ represents the horizontal friction), and vertical friction are collectively termed as D. N represents the effect by the nonlinear advection term. Finally, the subscripts e and i respectively represent the external and internal modes and it is straightforward to show that

$$N_i=A-N_e$$
$$B_i=G+B-B_e$$
$$W_i=W-W_e$$
$$D_i=D-D_e$$

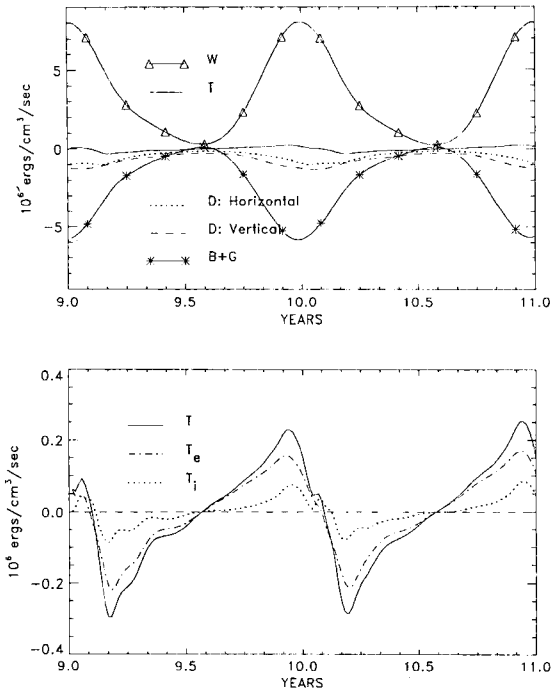

Fig. 12. The flat bottom ocean energy balance of the total kinetic energy (upper: see text for details) and decomposition of T into the external and internal modes (lower).

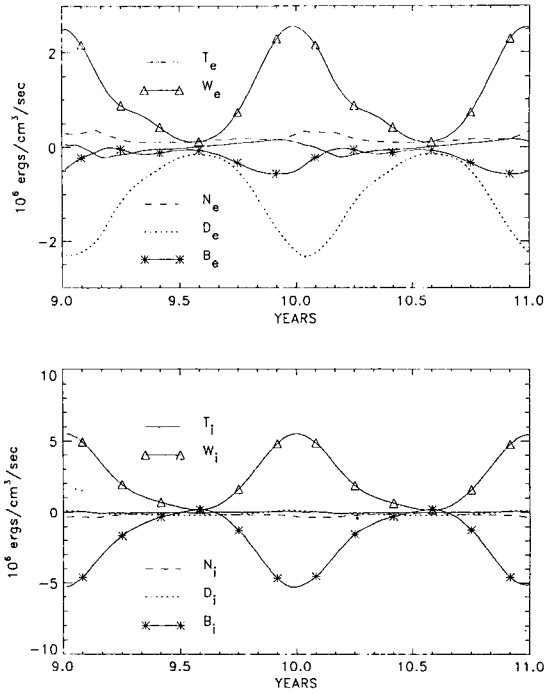

Fig. 13. The energy balance of the external (upper) and internal (lower) modes.

A and G become zero in a closed domain but represent the exchange of kinetic energy with the outside domain if integration is done in a limited domain. B is the energy conversion term between the kinetic energy and the potential energy. The energy flows from kinetic energy to potential energy when B is negative, i.e., when the vertical velocity w is positive. There are two routes of energy exchange between the external and internal modes; direct exchange through the nonlinear term N and indirect exchange via the energy conversion terms B_e and B_i.

The wind forcing (W), work done by pressure gradient force (G+B), dissipation (D), and time rate of change of total kinetic energy ($T \equiv \partial E/\partial t$) are displayed over 2 years of period (year 9-11) after the initial spin-up is accomplished (Fig. 12). Wind is the main source of the kinetic energy throughout the most of the year and is balanced by the work done by pressure gradient force (B+G) and the dissipation (D). The small net value resulting from the imbalance between them actually determines the time variation of the total kinetic energy. The wind forcing is always positive but the kinetic energy increases only when the wind forcing increases (July-January) according to Fig. 12. Most of the energy from the wind forcing is used to increase the potential energy of the ocean.

A close look reveals that the contribution by the external mode dominates the time rate of change of the total kinetic energy (Fig. 12). Since the external mode is the barotropic mode, the dominance of the barotropic mode in the time variation demonstrates that the transient ocean response in the absence of the topography is mainly barotropic. It suggests that the seasonal fluctuation in a flat-bottom ocean is large. The fast propagation speed of the barotropic Rossby wave and consequently the short spin-up time, only one month at most, makes the ocean response almost in phase with the forcing. Also, the amplitude of the response is large, especially in this flat-bottom case because there is no dissipation or scattering of the barotropic mode by to[redacted]hy. However, this [redacted]ld not be the case

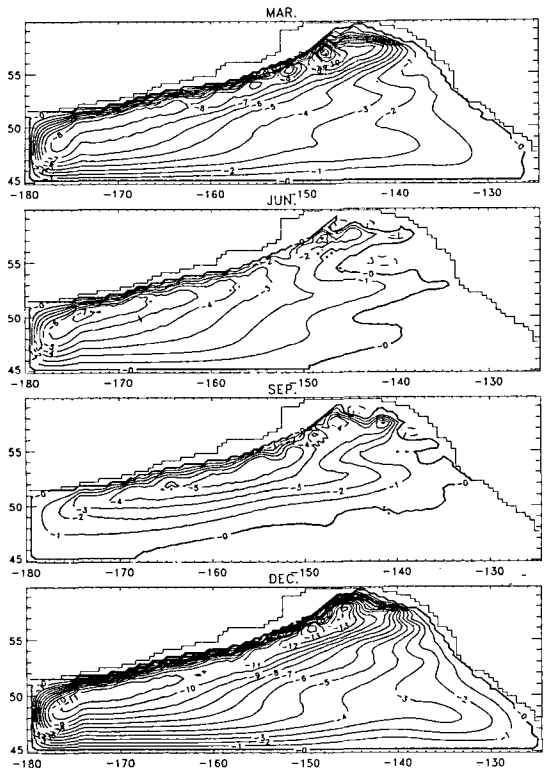

Fig. 14. Baroclinic model with flat topography stream function in March, June, September, and December from year 9.

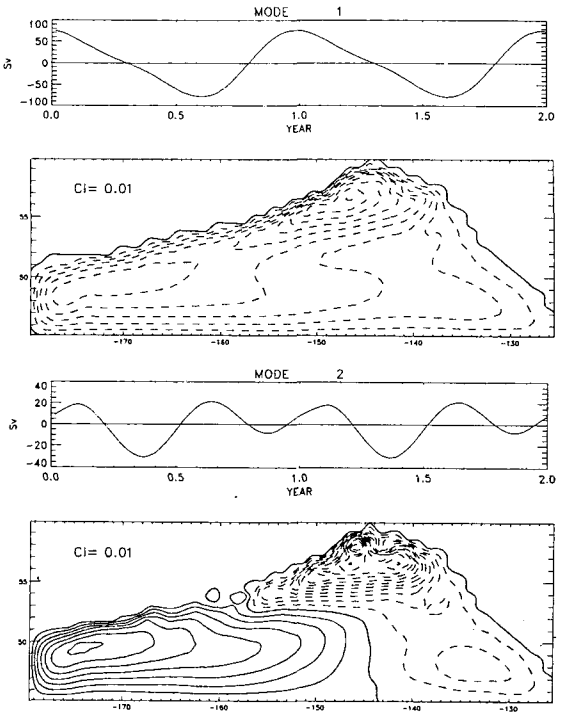

Fig. 15. Time functions and eigenvectors (CI: contour interval) of the first two EOF modes of year 9-11. The eigenvector is zero at the boundary.

near the equator where the propagation speed of the baroclinic Rossby wave is comparable to the barotropic Rossby wave. This result is also consistent with the theory that the ocean response to the seasonal forcing at middle and high latitudes is mainly barotropic (Anderson and Corry 1985a).

More detailed energy balances of the internal and external modes (Fig. 13) show that the major components maintaining the external mode are the wind (W_e) and the dissipation (D_e) while the wind (W_i) and the energy conversion term (B_i) are the major terms in the balance of the internal mode. Bottom friction is the dominant dissipative component of the external mode. About two thirds of the wind energy enters the ocean through the internal mode and most of the dissipation is done through the external mode. The nonlinear term shows an energy transfer om the internal mode to t ternal mode.

Seasonal cir a c linic m

14) shows a large seasonal variability similar to the seasonal barotropic model (Fig. 10). The cyclonic gyre covers the entire gulf in fall (December) and winter (March) but retreats to the west and north in other seasons. The zero stream function lines in spring (June) and summer (September) are at about the same position as the zero wind stress curl lines (Fig. 2). This confirms that the barotropic mode is the primary response in a flat-bottom ocean. Eddies are also seen in the westward flowing boundary current from 140° W to at least 160° W (Fig. 14).

An EOF analysis for the 2-year stream function data of year 9-11 (Fig. 15) shows that the seasonal forcing generates most of the fluctuations. The first mode, which fluctuates at annual frequency, explains 86.3% of all variance (Table 1). It is characterized by a quick rise and slow fall of the time function. The spatial pattern of the eigenvector resembles the mean cyclonic gyre and represents the cycle of intensification and weakening of cyclonic circulation through the year. The maximum amplitude

Table 1. Percentages explained by the first three EOF modes of stream function from year 9 to 11.

EOF Mode	Variance Explained	Cumulative %
1st	86.3	86.3
2nd	8.0	94.3
3rd	3.6	97.9

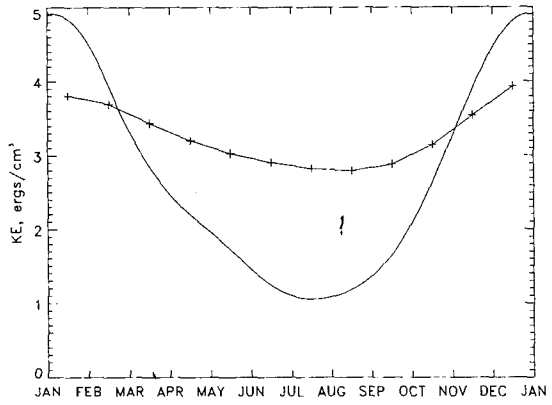

Fig. 16. Kinetic energy (ergs/cm³) of the baroclinic model with bottom topography for the upper 1,200 m of year 18-19 (+). Basin-averaged kinetic energy of the flat-bottom case is also shown for comparison (solid).

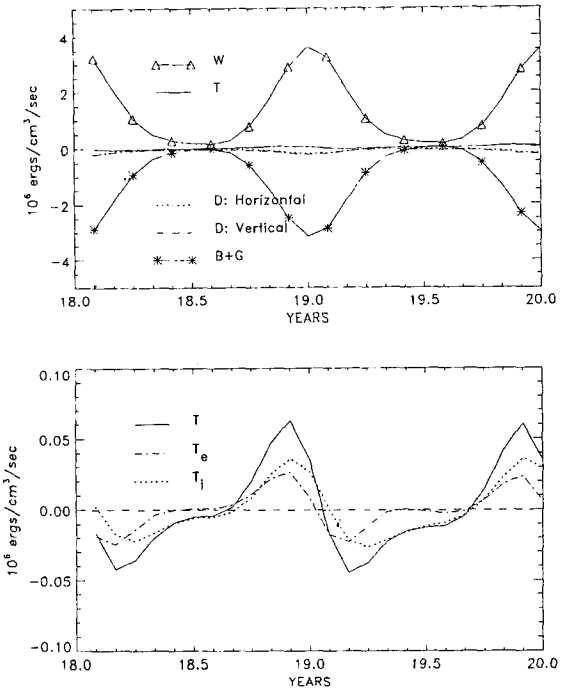

Fig. 17. The energy balance of the total kinetic energy (upper) and decomposition of the time rate of change (T) into the external and internal modes (lower).

of variation associated with the first mode is about 7 Sv (the contribution of each mode to the original data is time function×eigenvector, i.e., 80 from time function×0.09 from eigenvector of the first mode) at the center of gyre. The time function of the second mode fluctuates at semi-annual frequency and explains only 8% of the total variance. This mode displays a bimodal structure in space with a cyclonic gyre in the northeast half and an anticyclonic gyre in the southwest half and has a westward shift of the gyre during the spring and summer.

5.2 Topography Case

The introduction of the topography into the model radically changes the ocean's response to the seasonal wind forcing. The seasonal fluctuation of the kinetic energy is greatly reduced compared to the flat-bottom case (Fig. 16). This small response clearly shows the effect of the topography.

Decomposition of the total velocity into the external and internal modes is done to investigate the roles of each mode in the seasonal response (Fig. 17). The results show that both modes contribute more or less equally to the time variation of the total kinetic energy (T) unlike in the flat-bottom case where the external mode was dominant. The amplitude of T of the present case is only a quarter of that of the flat-bottom case and the energy reduction from the flat-bottom case is more severe in the external mode (T_e) than the internal mode (T_i). The external mode is reduced almost an order of magnitude (85%) while the internal mode is reduced by about 45%. Therefore, the presence of the topography has major impact on the external mode and the reduced role of the external mode in the topography case results in a small seasonal variability.

As in the flat-bottom case, most of the wind energy input to the ocean occurs through the internal mode (Fig. 18) and is balanced by the work by pre force (B_i). In the external mode, however, th (B_e) dor y ssure an important pograp s th rgy nd the dissi-

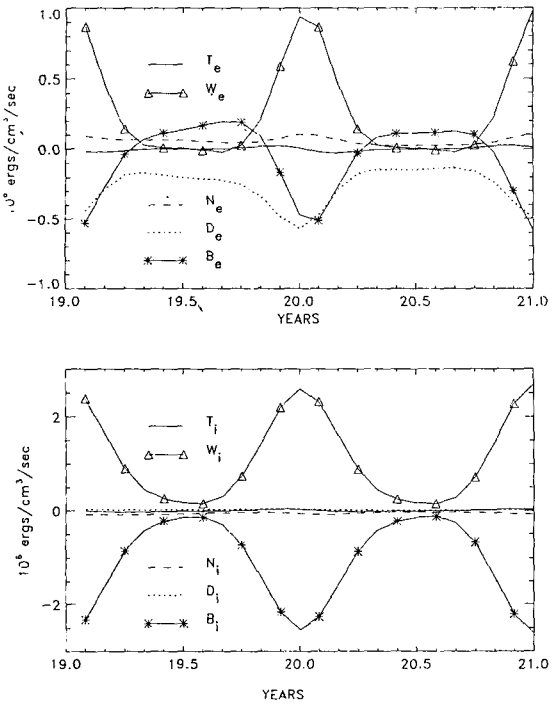

Fig. 18. The energy balance of the external (upper) and internal (lower) modes.

pation which were two major terms in the balance of the external mode of the flat-bottom case. In the topographic case, the rates of the wind energy input and the dissipation through the external mode are about 50% and 25% of the corresponding rates of the flat-bottom case, respectively. During the period of small wind energy input, a balance is achieved between B_e and D_e. This is in contrast to when the wind energy input is large when they balance W_e. Therefore, the external mode is driven by wind forcing from November through March and by pressure work (or energy release from potential energy) during the rest of the year. Holland (1975) also found that the external mode is maintained by B_e during the winter months when the wind forcing is weak there.

The seasonal variation of the transport is estimated by the range of the monthly mean stream function over one year of year 18-19 (Fig. 19). The seasonal range is [illegible] by the [illegible] of maximum [illegible] of str[illegible]on after a lin[illegible]

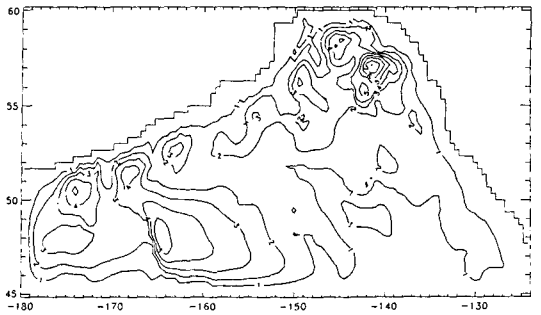

Fig. 19. The seasonal range of stream function (in Sv) from year 18-19 for the baroclinic model with bottom topography.

bution of the seasonal range resembles closely that of the seasonal barotropic model (Fig. 8) and no major differences in the pattern are found between these two figures except for their magnitudes. In general, the seasonal ranges of the baroclinic model are larger than those of the barotropic model but the differences are mainly found in those regions with large values.

The fact that the spatial pattern of the seasonal range of the baroclinic model is almost identical to that of the barotropic model suggests that the seasonal variation is mainly barotropic. One may argue that the stream function used for the determination of the seasonal range is a barotropic variable. But considering that a change in the density field would also cause changes in the stream function, the close similarity between the baroclinic model and barotropic model strongly indicates that there is little seasonal change in the density field. This in turn means that the seasonal variability in the Gulf of Alaska is primarily barotropic. No definitive seasonal variations are found in the seasonal circulation pattern (Fig. 20) except for an appearance of the anticyclonic circulation within a couple degrees of the southern boundary and the coast of North America south of 55° N in spring and summer. Thus the mean state changes little over the seasons. This is in contrast to Cummins (1989) where seasonal westward shift of the gyre is observed in his QG model. Based on this shift, Cummins (1989) further suggested that the abnormal shift of the Alaska gyre (Royer and Emery 1987) is the amplified version of the seasonal shift. However, the

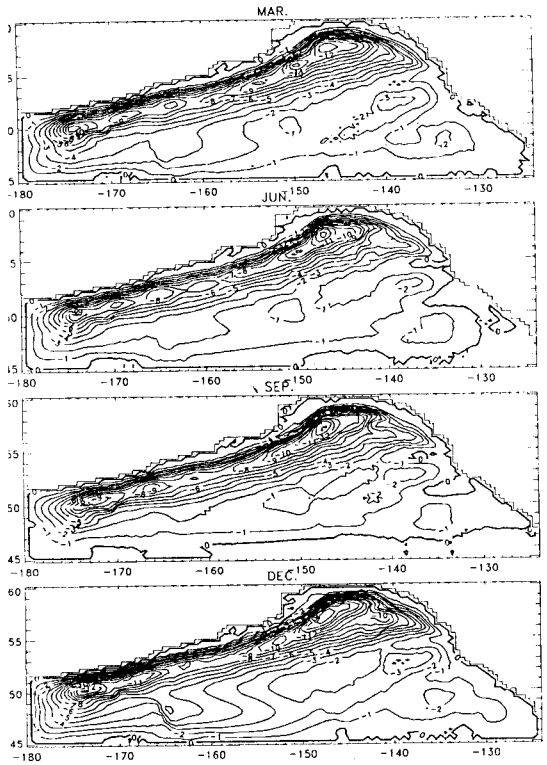

Fig. 20. Contour plots of stream function in March, June, September, and December from year 18.

absence of the seasonal westward shift of the gyre in the seasonal baroclinic model as well as in the diagnostic model (Fig. 3) suggests that the abnormal shift of the gyre is not due to the amplification of the seasonal phenomenon but due to the passage of the anticyclonic eddies originated from the Alaska Current region (Musgrave *et al.* 1992). Furthermore, a seasonal shift of the Alaska gyre is not likely to occur in nature considering that the estimate of the seasonal variations in the transport of the Alaska Stream is none to only 13% at most (Reed *et al.* 1980; Royer 1981).

6. DISCUSSION AND CONCLUSIONS

A series of numerical experiments has been carried out to simulate the ocean circulation in the Gulf of Alaska. Experiments have proceeded starting from very simple ones and gradually adding new features to increase their realism. A focus of this work is on the explanation of the seasonal variability of the Alaska Stream. The experiments began with a diagnostic model. Yearly average and seasonal circulations have been produced from observed density field. The derived picture agrees well (especially in the surface layer) with observations and measurements. An interesting result of this diagnostic model is the existence of permanent eddies south of the Alaska Stream.

The second experiment is a seasonal barotropic model with bottom topography which is forced by the time-varying wind stress. The resulting circulation is surprisingly weak due to the scattering effect of the bottom topography. This model is helpful in understanding the seasonal response of the seasonal baroclinic model because there are similarities in the spatial patterns of the seasonal range between the seasonal barotropic model and a later seasonal baroclinic model. It suggests that the seasonal response of the seasonal baroclinic model is mainly barotropic. Furthermore, the diagnostic model also shows a similar spatial pattern with the exception of the noise due to the mismatch between the density field and the bottom topography. Therefore, it is certain that the seasonal variability in the Gulf of Alaska is primarily barotropic and there is little seasonal variability in the density field.

As a final experiment, seasonal variability of the baroclinic model is studied. It was found that bottom topography greatly affects the ocean's response to the seasonal forcing. The seasonal circulation response in the flat-bottom case directly responds to the change in the wind stress curl while the seasonal variation in the topography case is not as well pronounced. Seasonal transport variations occur through both the external and internal modes in the topography case while the external mode is the major contributor in the flat-bottom case. This difference determines the baroclinic ocean response to the seasonal forcing because of the differences in the propagation speed and the spin-up time of these two modes. The dominance of the fast propagating barotropic mode (barotropic Rossby waves) accompanied by the absence of a scattering effect of bottom topography enables the flat bottom ocean to [illegible] as well as seasonal [illegible] is in cont-

rast to the reduced role of the barotropic mode and the scattering by bottom topography which makes the seasonal fluctuations small in a ocean with topography.

The non-topographic Sverdrup circulation is established in a flat-bottom ocean whether its stratification is barotropic or baroclinic. A major difference between the barotropic and baroclinic oceans is in the spin-up time for the establishment of the Sverdrup circulation. The barotropic Rossby waves which are solely responsible for the spin-up of the barotropic ocean propagate at a speed of on the order of 1 m/sec and the ocean reaches an equilibrium on the time scale of one month. On the other hand, first baroclinic Rossby waves are dominant in a baroclinic ocean and equilibrium is achieved only after their propagation to the western boundary, which takes a decade at a speed of on the order of 1 cm/sec at high latitudes.

When bottom topography is introduced into the model, the circulation differs significantly from the flat-bottom case. Bottom topography alters the circulation considerably in the barotropic ocean because the barotropic Rossby waves are now generated by $\mathrm{curl}_z\ (\tau/H)$ where τ is the wind stress and H is the ocean depth (Anderson and Corry 1985b). So, the effect of bottom topography directly influences the barotropic ocean. In a baroclinic ocean, however, the effect of topography is alleviated by the baroclinicity. The ocean forced by a constant wind forcing achieves the non-topographic Sverdrup circulation after the propagation of the baroclinic Rossby waves that compensate the effect of topography.

The situation is similar in the case with time-dependent forcing, or more specifically, seasonal forcing as with the constant forcing. Fast barotropic Rossby waves easily catch up with the time changes in the forcing and are fully represented in the ocean circulation. On the other hand, the baroclinic Rossby waves propagate only a small distance before temporal forcing changes occur. Consequently, the compensation of the topography is not complete over the entire ocean but is limited only near their generation re . Therefo n-topogr Sve- d not d. T sc t nc

the ocean response to the seasonal forcing is mainly barotropic at middle and high latitudes. Therefore, the response of the ocean with bottom topography to the seasonal forcing can be considered as the sum of barotropic response and the localized baroclinic response.

According to the diagnostic model, seasonal barotropic model and seasonal baroclinic model, the seasonal variation of the total transport in the Alaska Stream region is only 2 Sv. Since it is based on the stream function which represents the vertically integrated transport, an estimate of the seasonal variation in the upper 1,500 m is also made and is about 1 Sv. This value can be compared to the quantitative estimate by Royer (1981) which is based on 21 geostrophic current observations relative to 1,500 db between 148° W and 165° W. He estimated 13% as the seasonal amplitude relative to the mean transport of 9.2 Sv. Using these values, one can estimate the lower limit of the seasonal range as 2.4 Sv assuming no contribution from the deep layers (note that the seasonal range is twice the amplitude). Therefore, the estimate of 1 Sv as the seasonal range in the upper 1,500 m lies between the estimate 2.4 Sv of Royer (1981) and no seasonal variability of Reed *et al.* (1980).

The small seasonal variability in the transport, along with no appreciable seasonal variation in the circulation pattern, can be compared to the results of Cummins (1989) and Hsieh (1987). In Hsieh (1987), the seasonal fluctuation of the Alaska gyre appears to be similar to our flat-bottom model. His used of a small number of vertical levels causes this unrealistic circulation. This was also pointed out by Cummins (1989). However, a seasonal east-west shift of the Alaska gyre is also observed in Cummins (1989) which is not seen in the diagnostic and seasonal baroclinic models of this study. We believe that the prior shifts in the gyre as discussed in Royer and Emery (1987) are actually the result of a mesoscale eddy. Therefore, the large deep circulation of this high latitude baroclinic ocean is markably constant from season to season in spite an order of magnitude change in the wind forg through year.

REFERENCES

Anderson, D.L.T. and Corry, R.A., 1985a. Ocean response to low frequency wind forcing with application to the seasonal variation in the Florida Straits-Gulf Stream transport, *Prog. Oceanog.*, **14**, 7-40.

Anderson, D.L.T. and Corry, R.A., 1985b. Seasonal Transport Variations in the Florida Straits: A Model Study, *J. Phys. Oceanogr.*, **15**, 773-786.

Anderson, D.L.T. and Gill, A.E., 1975. Spin-up of a stratified ocean, with applications to upwelling, *Deep Sea Res.*, **22**, 583-596.

Anderson, D.L.T. and Killworth, P.D., 1977. Spin-up of a stratified ocean, with topography, *Deep Sea Res.*, **24**, 709-732.

Bang, I. and Kowalik, Z., 1994. A numerical modeling study of the interannual variability in the Gulf of Alaska, *J. Korean Soc., Coastal and Ocean Engineers*, Vol. 6(3), 298-308.

Bryan, K., 1969. A numerical method for the study of the ocean circulation, *J. Comput. Phys.*, **4**, 347-376.

Cummins, P.F., 1989. A quasi-geostrophic circulation model of the Northeast Pacific. Part II: Effects of topography and seasonal forcing, *J. Phys. Oceanogr.*, **19**, 1649-1668.

Favorite, F., Dodimead, A.J. and Nasu, K., 1976. Oceanography of the subarctic Pacific region, 1960-1971. International North Pacific Fisheries Commission Bulletin, 33.

Greatbatch, R.J. and Goulding, A., 1989. Seasonal Variations in a Linear Barotropic Model of the North Pacific Driven by Hellerman and Rosenstein Wind Stress Field, *J. Geophy. Res.*, **94**, 12645-12665.

Holland, W.R. 1975. Energetics of baroclinic oceans. *Numerical models of ocean circulation.*, National Academy of Sciences, 168-177.

Holland, W.R. and Hirschman, A.D., 1972. A numerical calculation of the circulation in the North Atlantic ocean, *J. Phys. Oceanogr.*, **2**, 336-354.

Hsieh, W.W., 1987. A numerical study of the seasonal cycle and its perturbations in the northeast Pacific Ocean, *Atmos. Ocean*, **25**, 375-386.

Levitus, S., 1982. Climatological atlas of the world ocean. NOAA Prof. Paper 13.

Lighthill, M.J., 1969. Dynamic Response of the Indian Ocean to Onset of the Southwest Monsoon, *Philosophical Transactions of the Royal Society of London*, **A 270**, 371-390.

Musgrave. D.L., Weingartner, T.J. and Royer, T.C., 1992. Circulation and hydrography in the northwestern Gulf of Alaska., *Deep Sea Res.*, **39**, 1499-1519.

Reed, R.K., 1968. Transport of the Alaska Stream, *Nature*, **220**, 681-682.

Reed, R.K., Muench, R.D. and Schumacher, J.D., 1980. On baroclinic transport of the Alaskan Stream near Kodiak Island, *Deep Sea Res.*, **27A**, 509-523.

Reid, J.L. and Arthur, R.S., 1975. Interpretation of maps of geopotential anomaly for the deep Pacific ocean, *J. Mar. Res., Supplement*, **33**, 37-52.

Reid, J.L. and Mantyla, A.W., 1976. The effect of geostrophic flow upon coastal sea elevations in the northern North Pacific ocean, *J. Geophy. Res.*, **81**, 3100-3110.

Royer, T.C., 1981. Baroclinic transport in the Gulf of Alaska. Part I. Seasonal variations of the Alaska Current, *J. Mar. Res.*, **39**, 239-250.

Royer, T.C. and Emery, W.J., 1987. Circulation in the Gulf of Alaska, 1981. *Deep Sea Res.*, **34**, 1361-1377.

Sarkisyan, A.S., 1966. *Theory and Computation of Ocean Currents*, Moscow, Gidrometeoizdat. (English translation IPST Press, Jerusalem 1969).

Sarkisyan, A.S. and Ivanov, V.F., 1971. Joint effect of baroclinicity and bottom relief as an important factor in the dynamics of sea currents, Ivz. Akad. Nauk SSSR, Fiz. Atmos. Okeana, 7, 173 (Engl. transl., p. 116).

Sarkisyan, A.S. and Pastukhov, A.F., 1970. The density field as the main indicator of steady sea currents, Ivz. Akad. Nauk SSSR, Fiz. Atmos. Okeana, 6, 64 (Engl. transl., p. 34).

Semtner, A.J., 1974. An oceanic general circulation model with bottom topography, Numerical Simulation of Weather and Climate, Tech. Rep. No. 9, Dept. Meteor. UCLA, 99p.

Veronis, G. and Stommel, H., 1956. The action of variable wind stresses on a stratified ocean, *J. Mar. Res.*, **15**, 43-75.

Warren, B.A. and Owens, W.B., 1988. Deep currents in the central Subarctic Pacific Ocean, *J. Phys. Oceanogr.*, **18**, 529-551.

Willebrand, J., 1978. Temporal and spatial scales of the wind field over North Pacific and North Atlantic, *J. Phys. Oceanogr.*, **8**, 1080-1094.